CHEMISTRY OF MATERIALS

pubs.acs.org/cm

Article

# The Roles of Citrate and Defects in the Anisotropic Growth of Ag Nanostructures

Heng Xu and Benjamin J. Wiley*

Cite This: *Chem. Mater.* 2021, 33, 8301−8311

Read Online

ACCESS | Metrics & More | Article Recommendations | Supporting Information

**ABSTRACT:** Synthetic control of nanocrystal shape is often achieved by controlling the crystal structure of the seed crystals as well as through the use of additives that are thought to block atomic addition to certain facets. However, the effect of the crystal structure or additives on the rate of atomic addition to a specific facet is not usually quantified, making it difficult to understand and design nanocrystal syntheses. This article combines single-crystal electrochemistry measurements with measurements of anisotropic nanocrystal growth to quantify the roles of citrate and planar defects in anisotropic atomic addition. Citrate lowers the rate of atomic addition to Ag(100) and Ag(111) single crystals by 3.2 and 15 times, respectively. Citrate decreases the rate of ascorbic acid oxidation in a facet-selective manner, but citrate decreases the rate of silver ion reduction to roughly the same extent on Ag(100) and Ag(111) single crystals. The degree to which citrate passivates single-crystal electrodes at different citrate concentrations closely matches the facet-dependent growth rates for single-crystal seeds. In contrast, seeds with planar defects exhibit anisotropic growth that is 30−100 times greater than can be explained by the facet-selective passivation by citrate. Without citrate, more silver deposits on the edges of seeds with planar defects than in the middle, but the seeds do not exhibit anisotropic growth. Evidence suggests that citrate improves the stability of nanoplates bounded by large {111} facets by preventing diffusion to {111} facets.

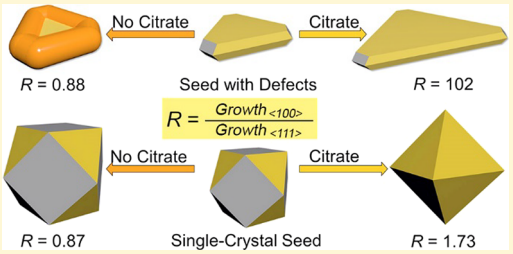




## INTRODUCTION

Silver nanocrystals are useful materials for catalysis,[1−5] surface-enhanced Raman scattering (SERS),[6−9] electronics,[10−12] and biomedical applications[13−15] due to their unique surface chemistry, excellent plasmonic properties, high conductivity, and good stability. The versatility of silver nanocrystals is due to the different nanocrystal shapes, and thus nanocrystal properties, that can be created with solution-phase syntheses. For example, the absorption of infrared light by silver nanoplates with high aspect ratios enables their use in photoacoustic imaging.[16,17] Long, thin silver nanowires are excellent materials for transparent conducting films because they reduce the cross-sectional area of silver required to achieve a conducting path while also reducing the light scattered per unit cross section.[18−23] Silver nanocubes and nanowires covered mostly by {100} facets exhibit higher catalytic selectivity for ethylene epoxidation than silver nanospheres covered mostly by {111} facets.[24,25] Silver nanooctahedra enclosed by {111} facets exhibit higher activity for plasmon-enhanced hydrogen evolution than silver nanocubes.[26] These examples demonstrate that shape-selective nanocrystal synthesis is critical for tuning the properties of silver nanocrystals so that these materials may be designed to solve a particular problem.

The primary means by which control of nanocrystal shape is achieved is through the addition of organic additives (e.g., citrate and PVP) or inorganic anions (e.g., $Cl^-$ and $Br^-$) to a solution phase synthesis.[27−35] One common hypothesis for the role of these additives is that they adsorb to and block atomic addition to certain facets.[28−31,35−44] Despite many previous mechanistic studies of nanostructure growth, it has proven difficult to provide a clear test of the capping agent hypotheses with synthetic studies alone.[28,40,45−47] The facet selectivity of a capping agent is often qualitatively deduced from the shape of metal nanocrystals formed in a synthesis. However, it is difficult to tell whether an additive is an activator or passivator from synthetic studies. For example, metal nanocubes could form as a result of an additive acting as a passivator of atomic addition to {100} facets or as an activator of atomic addition to {111} facets. The role of impurities, such as iodide in cetyltrimethylammonium bromide[31,48−53] or chloride in ethylene glycol,[28,54−56] can also complicate studies of the effect of additives on anisotropic growth. In many cases, there is no established quantitative relationship between the amount of capping agents added and the effect on the facet-selective rate of atomic deposition. Ideally, one could design a synthesis to

Received: July 16, 2021
Revised: October 6, 2021
Published: October 19, 2021




https://doi.org/10.1021/acs.chemmater.1c02474
*Chem. Mater.* 2021, 33, 8301−8311

produce a desired nanostructure shape, but the current understanding of the surface chemistry that results in a particular shape is not sufficient to enable such rational design. Instead, the development of metal nanostructure syntheses largely proceeds through trial and error.

Citrate is used as a reducing agent, colloidal stabilizer, and shape-directing agent in the synthesis of silver nanocrystals.[38,57,58] As citrate is usually used to produce silver nanocrystals enclosed by {111} facets, such as silver nanoplates, decahedra, and octahedra, it is thought that citrate is a capping agent for {111} facets, i.e., that it specifically adsorbs to {111} facets and prevents atomic addition.[33,38,58] Theoretical studies indicate that citrate has a higher binding affinity for {111} than {100} facets, supporting the capping agent hypothesis.[59,60] However, the degree to which citrate affects the rate of atomic addition to {111} or {100} facets has yet to be quantified. In some cases, citrate has been used to grow silver nanocrystals enclosed by {100} facets, specifically, pentagonally twinned nanorods from decahedral seeds.[58] In this case, the presence of twin defects may have promoted the observed anisotropic growth. Indeed, the presence of planar defects (twin planes and stacking faults) is thought to also contribute to the anisotropic growth of silver nanoplates grown with citrate.[61−63] It is at present unclear to what extent the anisotropic growth of structures such as nanoplates is caused by planar defects or capping agents such as citrate.

To quantify the roles of additives and defects in anisotropic growth, we rely on the fact that the process of metal nanocrystal growth is electrochemical. Metal nanostructure growth involves the oxidation of a reducing agent (e.g., ascorbic acid) and reduction of metal ions. Assuming that this redox process occurs at the surface of the metal nanostructures, the rate of this redox process can be determined by performing electrochemical measurements.[64] Electrochemical measurements with single crystal electrodes can be used to test hypotheses for the roles of organic additives and halides in nanostructure syntheses. These measurements have provided new insights. For example, ethylenediamine was found to promote copper nanowire growth by keeping the {111} facets on the ends of growing copper nanowires free of oxidation.[65] Hexadecylamine (HDA) was found to passivate both Cu(100) and Cu(111) surfaces equally, but adding chloride selectively displaced HDA from the {111} facets on the ends of nanowires, enabling anisotropic growth.[66] Addition of small concentrations of iodide to an HDA-mediated copper nanowire synthesis resulted in isotropic adsorption of iodide on both Cu(100) and Cu(111) but anisotropic growth of Cu microplates.[67] For the case of gold nanorods, bromide exhibited a facet-selective passivation of {100} facets, but cetyltrimethylammonium did not.[68]

Here we apply single-crystal electrochemistry to quantify how citrate affects the rate of atomic addition to the {111} and {100} facets of silver. We then use this result to determine the extent to which planar defects promote the anisotropic growth of silver nanoplates. We find that citrate is indeed a passivator of atomic addition to {111} and {100} facets and that it passivates {111} facets to a greater extent (by 3.4 times) than {100}. Surprisingly, the facet-selective passivation of {111} facets is entirely due to the effect of citrate on ascorbic acid oxidation; citrate has no facet-selective effect on silver ion reduction. The ratio of atomic addition to Ag(100) relative to Ag(111) single crystals at different citrate concentrations is closely corroborated by the rate of atomic addition to the {100} and {111} facets to silver cuboctahedra seeds. In contrast, seeds with planar defects exhibit a rate of anisotropic growth 30−100 times higher than can be explained by the facet-selective passivation of citrate. Without citrate, seeds with planar defects had thicker edges but did not exhibit anisotropic growth. We present evidence that suggests that planar defects catalyze the deposition of silver atoms while citrate prevents the diffusion of silver atoms to {111} facets, resulting in a rate of anisotropic growth 1−2 orders of magnitude greater than with single crystals.

## EXPERIMENTAL SECTION

**Materials.** A polycrystalline silver electrode (3.0 mm in diameter), a silver−silver chloride reference electrode (1 M KCl), and a platinum counter electrode were purchased from CH Instruments. Single-crystal silver electrodes were made from single-crystal silver disks (3.0 mm in diameter) purchased from Princeton Scientific. Each silver disk was first attached to a copper wire from one of the disk's flat round surfaces with a conductive silver epoxy adhesive (Epoxy International). The connected silver disk and copper wire were mounted in a polyether ether ketone (PEEK) sheath with a thermally conductive and electrically insulating compound (Strong-Bond 53, Epoxy International). The single-crystal electrodes were left to cure at room temperature for at least 24 h before use.

Ethylene glycol (EG, 99%) was obtained from J.T. Baker. Acetone and perchloric acid ($HClO_4$, 70%) were obtained from VWR Chemicals BDH. Silver trifluoroacetate ($CF_3COOAg$, 98%), sodium trifluoroacetate ($CF_3COONa$, 98%), L-ascorbic acid (AA, 99%), sodium citrate dihydrate ($Na_3CA{\cdot}2H_2O$, 99%), trifluoroacetic acid ($CF_3COOH$, 99%), polyvinylpyrrolidone (PVP, MW = 29,000), and polyvinylpyrrolidone (PVP, MW = 55,000) were obtained from Sigma-Aldrich. Silver nitrate ($AgNO_3$), citric acid ($H_3CA$, 99%), and sodium chloride (NaCl) were obtained from Fisher Chemical. Sodium hydroxide (NaOH), sodium borohydride ($NaBH_4$), and hydrogen peroxide ($H_2O_2$, 30%) were obtained from EMD Millipore. Ammonium hydroxide ($NH_4OH$, 50%) was obtained from Beantown Chemical. Hydrochloric acid (HCl, 37%) and sodium sulfide nonahydrate ($Na_2S{\cdot}9H_2O$, 98%) were obtained from Acros Organics. Chromium(VI) oxide ($CrO_3$, 99%) and sodium sulfate ($Na_2SO_4$, 99%) were obtained from Alfa Aesar. All the chemicals were used without further purification.

**Synthesis of Single-Crystal Truncated Nanocubes.** The synthesis of single-crystal seeds was based on a previous method with modifications.[54] First, 5 mL of ethylene glycol was added to a 250 mL double-neck flask preheated at 160 °C with a 20 cm condenser. A light nitrogen gas flow was applied above the solution for 10 min followed by heating for another 50 min. After this, 3 mL of a solution containing 94 mM $AgNO_3$ in EG and 3 mL of a solution containing 144 mM of PVP (MW = 55,000) and 0.22 mM of NaCl in EG were simultaneously added to the flask at a rate of 45 mL/h. The reaction solution turned yellow immediately after the addition of the two solutions and gradually turned clear within 1 h. The reaction solution turned light yellow again at about 5 h and gradually became a dark yellow color during the next 10 h. At 16 h, the reaction solution turned dark brown, gradually became greenish and finally turning ochre at 17 h, indicating that the reaction was complete. The exact completion time of the reaction can vary between 14 and 20 h. The reaction was quenched in an ice-water bath, 22 mL of acetone was added to the reaction solution, and this mixture was centrifuged for 30 min. The precipitate was washed with 10 mL of deionized water three additional times before it was dispersed in 5 mL of deionized water. The multiple washing steps ensured that the concentration of either PVP or EG in the seed solution was less than 1 nM. The single-crystal seeds were stored in a capped glass vial for less than 2 months before they were used for seed-mediated growth. We did not observe any changes in the shape or surface roughness of the single-crystal seeds over this 2 month period. Single-crystal seeds were previously found to be stable in water for 3 months.[69,70]


https://doi.org/10.1021/acs.chemmater.1c02474
Chem. Mater. 2021, 33, 8301−8311

**Synthesis of Nanodisks.** The synthesis of silver nanodisks was based on previous publications with slight modifications.[38] To start, 3 mL of a 30 mM sodium citrate solution, 3 mL of a 20 mg/mL PVP (MW = 29,000) solution, 120 μL of hydrogen peroxide (30%), and 1 mL of a 5 mM silver nitrate solution were sequentially added to 49 mL of deionized water in a beaker while stirring. After adding 1.2 mL of a 100 mM solution of sodium borohydride in water, the color of the reaction solution immediately turned yellow. The reaction then turned orange, brown, dark green, and finally blue after stirring for 90 min. The solution was stirred for an additional 10 min after the final color change. The product was then collected as a precipitate by centrifuging the solution at 10,000 rpm for 30 min. The product was washed with 10 mL of water two times and dispersed in 2 mL of deionized water. The product was used for the synthesis of silver nanoplate seeds within 1 day.

**Synthesis of Nanoplate Seeds.** The silver nanoplate seeds were grown from silver nanodisks. To start, 10 mL of a 2.4 mM ascorbic acid solution, 10 mL of a 3 mM sodium citrate solution, 9 mL of deionized water, and 1 mL of an as-prepared silver nanodisk solution were stirred in a 200 mL beaker. After stirring for 10 min, 10 mL of a solution containing 9 mM trifluoroacetic acid and 4.5 mM sodium sulfate was added to slow down the reaction and generate more uniform nanoplates. The solution was stirred for another 1 min. Following this, 20 mL of a solution containing 0.6 mM silver trifluoroacetate was added. The solution underwent a purple−blue−green−purple−blue color transition, and the reaction was stopped at 13 min. The solution was centrifuged at 10,000 rpm for 4 min. The precipitate was washed with 5 mL of deionized water and centrifuged at 10,000 rpm for 4 min two times. The precipitate was dispersed in 5 mL of deionized water and used as silver nanoplate seeds. The silver nanoplate seeds were used within 1 day for seed-mediated growth to avoid their transformation into quasi-spherical particles.

**Seed-Mediated Growth.** The seed-mediated growth of single-crystal seeds or seeds with planar defects was done in the same manner. For a typical synthesis with 0.45 mM citrate, 2 mL of a 2.4 mM ascorbic acid solution, 2 mL of a 2.7 mM sodium citrate solution, 2 mL of a 1.15 mM trifluoroacetic acid solution, and 2 mL of the seed suspension were first mixed. For the seed suspension containing truncated silver nanocubes, 0.05 mL of as-prepared seeds was diluted to 2 mL with water. For the seed suspension containing silver nanoplates, 0.5 mL of as-prepared seeds was diluted to 2 mL with water. Following the initial mixing step, 4 mL of a 0.6 mM silver trifluoroacetate solution was added. The solution was stirred for 13 min and then centrifuged at 10,000 rpm for 4 min. The precipitate was washed with 5 mL of deionized water twice and centrifuged at 10,000 rpm for 4 min. The product was dispersed in 0.5 mL of deionized water for imaging. For syntheses with other citrate concentrations, the preparation of the growth solutions can be found in Table S1. As the pH has an effect on the reducing power of ascorbic acid[71] and thus the growth rate, the concentration of trifluoroacetic acid was changed for different citrate concentrations to keep the pH = 3.6.

**Surface Diffusion on Silver Nanoplates.** The silver nanoplates for surface diffusion experiments were grown from silver nanodisks. To start, 10 mL of a 2.4 mM ascorbic acid solution, 5 mL of a 0.12 mM citric acid, 5 mL of a 360 mM PVP (MW = 29,000) solution, 5 mL of an 11.88 mM sodium trifluoroacetate solution, 5 mL of a 1.92 mM trifluoroacetic acid solution, 8 mL of deionized water, and 2 mL of an as-prepared silver nanodisk solution were stirred in a 200 mL beaker. Following this, 20 mL of a solution containing 0.6 mM silver trifluoroacetate was added. The solution was stirred for 13 min and then centrifuged at 10,000 rpm for 4 min. The precipitate was washed with 6 mL of deionized water and centrifuged at 10,000 rpm for 4 min four times. The precipitate was dispersed in 5 mL of deionized water for surface diffusion experiments.

The surface diffusion experiments were done under the same conditions as the seed-mediated growth except for the difference in temperature and the absence of silver ions. To start, 0.25 mL of the as-prepared silver nanoplate suspension was mixed with two different solutions. One solution contained 0.4 mM AA, 0.25 mM trifluoroacetic acid, and 0.9 mM sodium trifluoroacetate, while the other contained 0.4 mM AA, 1.15 mM trifluoroacetic acid, and 0.45 mM sodium citrate. The concentrations of trifluoroacetic acid and sodium trifluoroacetate were changed for different citrate concentrations to keep the pH = 3.6. The suspensions were heated in a water bath at 95 °C for 10 min and then centrifuged at 10,000 rpm for 4 min. The precipitate was washed with 3 mL of deionized water twice and centrifuged at 10,000 rpm for 4 min. The product was dispersed in 0.2 mL of deionized water for imaging.

**Scanning Electron Microscopy (SEM).** SEM images were obtained with an Apreo S scanning electron microscope (ThermoFisher Scientific) operated at an accelerating voltage of 2.0 kV and a beam current of 25 pA. The samples were prepared by dropping 2−10 μL of the sample solutions on a piece of silicon followed by drying in air.

**Transmission Electron Microscopy (TEM).** TEM images were obtained with an FEI Tecnai $G^2$ Twin operated at an accelerating voltage of 160 kV. Samples were prepared by dropping 12 μL of the sample solution on 300 mesh carbon-coated copper grids (Pacific Grid-Tech). The excess solution was removed with filter paper after 1 min, and the grid was dried in air before imaging.

**Electrochemical Measurements.** A polycrystalline silver electrode (3 mm in diameter) was mechanically polished with alumina powder (0.3 μm) to a mirror-like surface before each measurement. The single-crystal silver electrodes were prepared with a modified etching method.[72] The Ag(100) and Ag(111) electrodes (3 mm in diameter) were first mechanically polished with alumina powder (0.3 μm) until they appeared to have mirror-like surfaces. Then, each of the electrodes was dipped in three stirred solutions: (1) chromium trioxide (0.15 M) and hydrochloric acid (0.1 M) for 1 min, (2) ammonium hydroxide (50% v/v in water) for 5 min, and (3) perchloric acid (4 M) for 5 min. The electrodes were thoroughly rinsed with a flow of deionized water and dried with a flow of nitrogen gas after etching in each solution. The reliability of the etching method was verified by comparing features of underpotential deposition of $HS^-$ (Figure S1).[73] This was performed by purging a solution containing 0.75 mM sodium sulfide and 0.2 M sodium hydroxide with a light flow of nitrogen gas for 5 min. A polished single-crystal silver electrode was dipped into the solution with a Ag/AgCl reference electrode (1 M KCl) and a platinum wire counter electrode. Cyclic voltammetry (CV) measurements were performed between −1.50 and −0.75 V at a rate of 200 mV/s for the Ag(100) electrode and between −1.30 and −0.8 V at a rate of 100 mV/s for the Ag(111) electrode. As shown in Figure S1, oxidation of the $HS^-$ occurred only on Ag(111) but not on Ag(100).

The facet selectivity of citrate was measured by performing linear sweep voltammetry (LSV) in the growth solution for the seeds. The seed-mediated growth occurred too quickly for electrochemical analysis of the mixed reaction solution (the reaction was complete in 13 min), so the rates of silver ion reduction and ascorbic acid oxidation at the mixed potential were analyzed separately, i.e., in solutions containing no ascorbic acid or no silver ions, respectively. LSV was performed from 0.1 to 0.35 V at a rate of 5 mV/s with one polished single-crystal silver electrode as a working electrode, an Ag/AgCl electrode (1 M KCl) as a reference electrode, and a platinum wire as a counter electrode. Each solution was stirred for 2 min before the electrodes were placed into the solution, and the electrodes were held in the solution for 2 min before starting the LSV scan. The solutions were constantly stirred at 500 rpm during the measurement. The concentrations of additives in the solutions that were analyzed are summarized in Table S2.

**UV−Vis−NIR Spectroscopy.** The UV−vis−NIR spectra of silver nanocrystals were measured in aqueous solutions with a Shimadzu UV-3600 spectrophotometer. The single-crystal silver nanocrystals were diluted to an absorbance of around 0.5, while the silver nanoplates were diluted to an absorbance of around 0.25.


https://doi.org/10.1021/acs.chemmater.1c02474
Chem. Mater. 2021, 33, 8301−8311

## RESULTS AND DISCUSSION

**Effect of Citrate on the Shape of Single-Crystal Ag Nanoparticles.** To investigate how citrate affects the rate of atomic addition to different facets of a silver nanostructure, we focus on seed-mediated growth to isolate the effects of additives on anisotropic growth from their effects on nucleation. We start with the seed-mediated growth of single-crystal nanoparticles enclosed primarily by {111} and {100} facets to rule out effects from planar defects on anisotropic growth. Depending on the ratio ($R$) of growth along the <100> relative to the <111> direction $\left(R = \frac{\text{Growth}_{<100>}}{\text{Growth}_{<111>}}\right)$, single-crystal seeds will grow into single-crystal nanoparticles with different shapes, including cubes, truncated cubes, cuboctahedra, truncated octahedra, and octahedra (Figure 1).[36] Thus, one can use the final shape produced by seed-mediated growth as an indicator of the ratio of atomic addition to {111} and {100} facets.

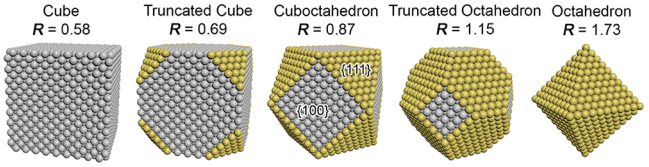


**Figure 1.** Schematic representation of single-crystal nanoparticles formed at different ratios ($R$) of growth along the <100> relative to the <111>. Cubes enclosed by square {100} facets form when $R$ = 0.58. Truncated cubes enclosed by octagonal {100} facets and triangular {111} facets form when $R$ = 0.69. Cuboctahedra enclosed by square {100} facets and triangular {111} facets form when $R$ = 0.87. Truncated nanooctahedra enclosed by square {100} facets and hexagonal {111} form when $R$ = 1.15. Octahedra enclosed by triangular {111} facets form when $R$ = 1.73.

Our starting seeds were a mixture of truncated cubes and cuboctahedra (see Figure 2A and Figure S2). In the absence of citrate (Figure 2B), almost all the seeds grew to form cuboctahedra with square {100} facets and triangular {111} facets, indicating an $R$ of about 0.87. In contrast, seeds grew to form octahedra in the presence of 0.45 mM citrate (Figure 2C), indicating an $R$ equal to or larger than 1.73.

The diameter $d$ of the truncated nanocubes and nano-octahedra was measured along the <100> direction after seed-mediated growth to quantify the extent of atomic addition to the {100} facets. Figure S3 illustrates how $d$ was defined for each shape. Without citrate, $d$ increased by 11.4 nm (from 64.5 ± 6.9 to 75.9 ± 8.0 nm). With 0.45 mM citrate, $d$ increased by 67.3 nm (from 64.5 ± 6.9 to 131.8 ± 18.8 nm). The larger increase in $d$ for the 0.45 mM citrate solution further illustrates that the deposition of silver atoms is more favorable on {100} facets than {111} facets with citrate. The synthetic results demonstrate that the presence of 0.45 mM citrate can increase $R$ for silver nanocrystals, but the value of $R$ determined from the nanocrystal shape is approximate, and this means of approximating $R$ does not provide any insights into how citrate affects the facet-selective rate of atomic deposition.

We performed surface diffusion experiments to verify if the anisotropic growth of octahedra in 0.45 mM citrate was kinetically controlled by the facet-dependent rate of atomic deposition rather than thermodynamically controlled by surface diffusion. The single-crystals seeds were stirred in the following three solutions: (1) 0.45 mM $Na_3CA$, (2) 0.45 mM $Na_3CA$ with 0.4 mM AA, and (3) 0.45 mM $Na_3CA$ with 0.2 mM $Ag^+$. After stirring for 13 or 120 min, no changes in shape were observed (see Figure S4). This result indicates that the anisotropic growth was due to a difference in the rate of atomic deposition between {100} and {111} facets.

**Effect of Citrate on the Facet-Selective Electrochemistry of Ag.** We performed measurements on Ag(100)

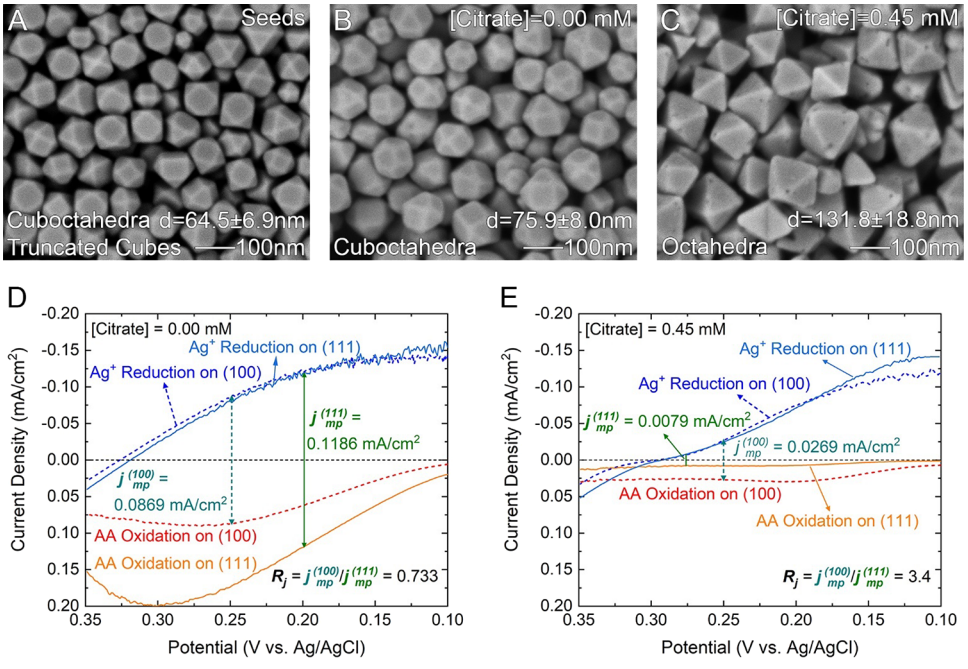


**Figure 2.** (A) SEM image of single-crystal silver seeds. (B) SEM image of the silver cuboctahedra grown from seeds with no citrate. (C) SEM image of octahedra grown from seeds with 0.45 mM citrate. LSV of the half-reactions on Ag(100) and Ag(111) electrodes in (D) 0.00 mM and (E) 0.45 mM citrate.


https://doi.org/10.1021/acs.chemmater.1c02474
Chem. Mater. 2021, 33, 8301−8311

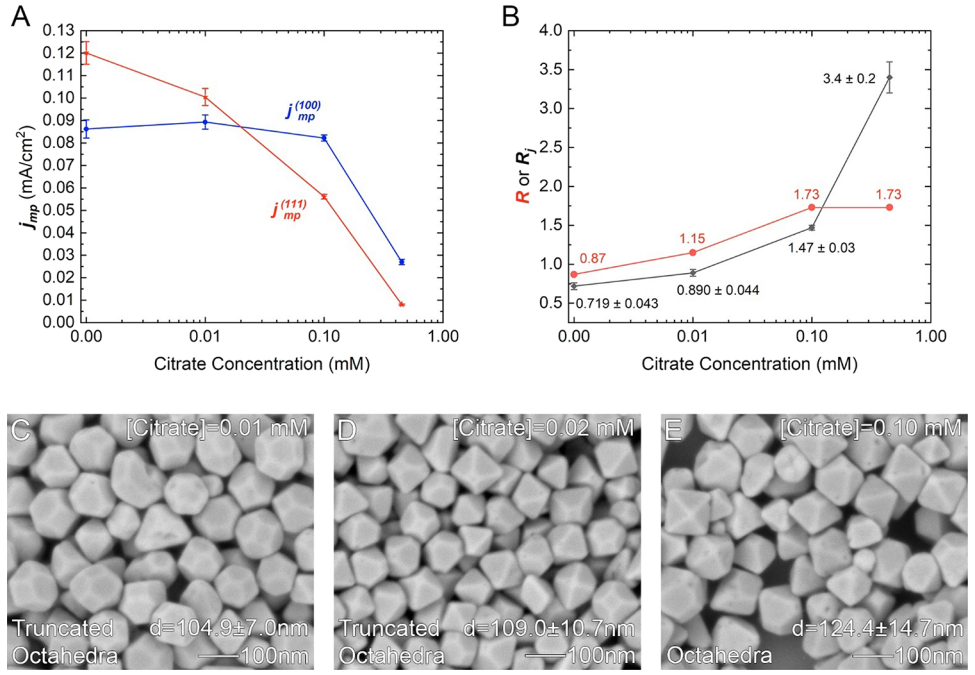


**Figure 3.** (A) $j_{mp}^{(100)}$ and $j_{mp}^{(111)}$ at different citrate concentrations. (B) $R$ (growth along <100>/<111>) and $R_j$ ($j_{mp}^{(100)}/j_{mp}^{(111)}$) at different citrate concentrations. (C–E) SEM images of the silver nanocrystals grown from the single-crystal seeds at citrate concentrations of (C) 0.01 mM citrate, (D) 0.02 mM citrate, and (E) 0.10 mM citrate.

and Ag(111) single-crystal silver electrodes to provide a more quantitative measurement of the effects of citrate on the rate of atomic addition to different facets. The single-crystal electrodes are used as models for the reactions occurring on the {100} and {111} facets of the silver seeds. We assume that the overall reaction for seed-mediated growth can be separated into two half-cell reactions: (1) reduction of silver ions: $2Ag^+ + 2e^- \rightleftharpoons 2Ag$ and (2) oxidation of AA to dehydroascorbic acid (DHA): AA → DHA + $2H^+$ + + $2e^-$.[71] Assuming that no other electrochemical reactions are taking place, the current from these two reactions occurring spontaneously in the reaction flask must be equal and opposite so as to avoid the accumulation of charge. The electrochemical potential at which these two reactions are equal and opposite is called the mixed potential ($E_{mp}$).[74] At the mixed potential, the overall current is zero because the two reaction currents are equal and opposite. However, one can measure the current density ($j_{mp}$) for either half-reaction at the mixed potential to determine the overall reaction rate. For spontaneous electrochemical reactions that are relatively slow, the $j_{mp}$ can be extracted from a Tafel plot of (log|$j$| vs E) obtained from the mixed reaction solution.[66−68] The seed-mediated growth studied in this paper occurred too quickly for electrochemical analysis of the mixed reaction solution (the reaction is complete in 13 min), so we analyzed the two half-cell reactions separately. We compared reaction rates on Ag(100) and Ag(111) surfaces to measure how citrate affects the facet selectivity of the half-reactions. The process for obtaining the current densities for the two half-reactions at the mixed potential is described in more detail in the Supporting Information and Figure S5.

In the absence of citrate, the $j_{mp}$ on the Ag(100) electrode ($j_{mp}^{(100)}$) is 0.0869 mA/cm$^2$ and the $j_{mp}$ on the Ag(111) electrode ($j_{mp}^{(111)}$) is 0.1186 mA/cm$^2$, so the ratio ($R_j$) of $j_{mp}^{(100)}/j_{mp}^{(111)}$ without citrate is 0.733 (Figure 2D). This value is close to the estimated $R$ value of 0.87 from the analysis of the nanocrystal shape (Figure 2B). With 0.45 mM citrate, the $j_{mp}^{(100)}$ is 0.0269 mA/cm$^2$ and the $j_{mp}^{(111)}$ is 0.0079 mA/cm$^2$, giving an $R_j$ of 3.4 (Figure 2E). This value is larger than 1.73 and therefore is sufficient to produce octahedra, as was observed from the synthetic results (Figure 2C). Note that 0.45 mM citrate reduced the $j_{mp}$, and thus the rate of the reaction, on Ag(100) by 3.23 times and on Ag(111) by 15.0 times. Thus, we confirm that citrate is a facet-selective capping agent.

We performed additional electrochemical measurements and seed-mediated syntheses at an intermediate range of citrate concentrations (0.01, 0.02, and 0.1 mM) to further examine the relationship between nanocrystal shape and $j_{mp}^{(100)}/j_{mp}^{(111)}$. The results from LSVs in Figure S6 are summarized in Figure 3A. Figure 3A shows that $j_{mp}^{(100)}$ remained fairly constant at citrate concentrations of 0.1 mM or lower but decreased by a factor of 3 when the citrate concentration was increased to 0.45 mM. This result indicates that relatively high concentrations of citrate are required to passivate the Ag(100) surface. In contrast, $j_{mp}^{(111)}$ decreases across the entire range of citrate concentrations, indicating that Ag(111) is more susceptible to passivation by citrate.

Figure 3B compares $R_j$ (i.e., $j_{mp}^{(100)}/j_{mp}^{(111)}$) to the value of $R$ determined by analyzing the nanocrystal shape produced at each concentration of citrate (Figure 3C–E). UV–vis–NIR spectra for the nanostructure product at different citrate concentrations are given in Figure S7A. Growth at a citrate concentration of 0.01 mM yielded truncated octahedra with square {100} facets and hexagonal {111} facets, indicating an $R$ of 1.15 (Figure 3C). A citrate concentration of 0.02 mM yielded slightly truncated octahedra, indicating an $R$ between 1.15 and 1.73 (Figure 3D). The 0.10 mM citrate solution yielded mostly octahedra, indicating an $R$ of 1.73 (Figure 3E).

These values of $R$ agreed remarkably well with the value of $R_j$ determined from the electrochemical experiments. For comparison, in the synthesis of pentagonally twinned copper nanowires, the aspect ratio of the nanowires was 400, but $j_{mp}^{111}/j_{mp}^{110}$ was 14.7.[66] Likewise, in the synthesis of pentagonally


https://doi.org/10.1021/acs.chemmater.1c02474
Chem. Mater. 2021, 33, 8301−8311

twinned gold nanorods, the aspect ratio of the nanorods was about 16 when the ratio of $j_{mp}^{111}/j_{mp}^{110}$ was about 1.4.[68] In both of these cases, the ratio of $j_{mp}^{111}/j_{mp}^{110}$ was more than 10 times lower than that necessary to explain the aspect ratio of the synthesized nanostructures. However, in the case of seed-mediated growth of the single crystals, $R_j$ was only about 0.22 smaller than $R$ between 0.00 and 0.10 mM citrate. The large differences between the aspect ratio and facet-selective electrochemical results observed in the previous work may be due to the presence of twin defects on the nanocrystals promoting anisotropic growth. This possibility is examined in more detail below.

**Ascorbic Acid Oxidation but Not $Ag^+$ Reduction Is Selectively Blocked by Citrate on Ag(111).** The single-crystal electrochemical measurements provide new insights into how citrate reduces the rate of the reaction on {111} relative to {100}. Surprisingly, citrate does not reduce the rate of $Ag^+$ reduction in a facet-selective manner. Figure 2E shows that the current from $Ag^+$ reduction on Ag(100) and Ag(111) is almost identical. In contrast, the AA oxidation on Ag(111) is reduced to a much greater extent than on Ag(100). This means that changes in nanocrystal shapes upon the addition of citrate are caused by citrate decreasing the rate of AA oxidation to a greater extent on {111} than {100} facets.

Figure 4 further illustrates the effect of citrate on $Ag^+$ reduction and AA oxidation across a range of concentrations. To facilitate visualization, the current density from $Ag^+$ reduction or AA oxidation with citrate ($j^{Ag^+}$ or $j^{AA}$) was normalized by the current density from $Ag^+$ reduction or AA oxidation without citrate ($j_0^{Ag^+}$ or $j_0^{AA}$). Figure 4A shows that when the concentration of citrate is increased from 0.01 to 0.45 mM, $j^{Ag^+}/j_0^{Ag^+}$ decreases on both Ag(100) and Ag(111), indicating that citrate suppresses $Ag^+$ reduction. However, the values of $j^{Ag^+}/j_0^{Ag^+}$ are nearly the same on Ag(100) and Ag(111), indicating that citrate does not suppress $Ag^+$ reduction in a facet-selective manner. This is in contrast to $j^{AA}/j_0^{AA}$ for Ag(100) and Ag (111) in Figure 4B. On Ag(100), $j^{AA}/j_0^{AA}$ is around 1.0 at citrate concentrations of 0.01 and 0.10 mM, indicating no suppression of AA oxidation, but decreases to around 0.4 at a higher citrate concentration of 0.45 mM. For Ag(111), $j^{AA}/j_0^{AA}$ decreases dramatically from 0.8 to around 0.05 as the concentration of citrate is increased from 0.01 to 0.45 mM. This shows that AA oxidation on Ag(111) is much more easily suppressed by citrate than on Ag(100).

Based on these electrochemical results, we conclude that the anisotropic growth of silver cuboctahedra into octahedra is due to citrate selectively suppressing AA oxidation on {111} facets. The suppression of AA oxidation on {111} facets apparently decreases the number of electrons available for $Ag^+$ reduction on {111} facets, resulting in a reduced rate of silver deposition along the <111> direction. This result is somewhat surprising because if electrons from AA oxidation were able to travel through the seed crystals to different facets, then the facet-selective passivation of AA oxidation without the facet-selective passivation of $Ag^+$ reduction should not cause anisotropic growth. This result implies that the oxidation of AA is coupled to the reduction of $Ag^+$ at the surface of the seeds by, for example, $Ag^+$ taking part in the oxidation of AA or by excess $Ag^+$ ions immediately consuming electrons from AA oxidation on the same facet.

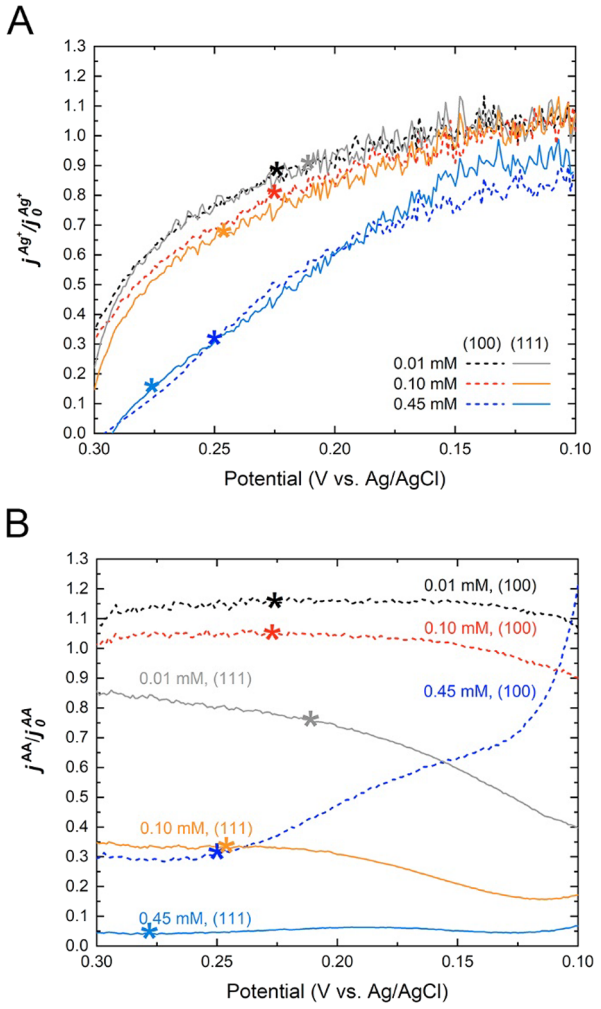


**Figure 4.** (A) Ratio of the current density from $Ag^+$ reduction with ($j^{Ag^+}$) and without citrate ($j_0^{Ag^+}$). (B) Ratio of the current density from AA oxidation with ($j^{AA}$) and without citrate ($j_0^{AA}$). The mixed potential is indicated with an asterisk.

An additional insight we can glean from these results is that the anisotropic growth of silver nanostructures in this synthesis is not due to the formation of a complex between citrate and $Ag^+$. It has been hypothesized that capping agents, such as citrate, can potentially cause anisotropic growth by forming a complex with $Ag^+$.[61,75,76] Although citrate may form a complex with $Ag^+$ in this reaction, the electrochemical results showing that citrate suppresses AA oxidation indicate that citrate adsorbs to the surface of silver. The fact that citrate does not affect $Ag^+$ reduction in a facet-selective manner indicates that if citrate does complex with $Ag^+$, such complexation is not the cause of anisotropic growth.

**Effects of Planar Defects on Anisotropic Growth.** Silver seeds can also contain planar defects such as twin boundaries and stacking faults. To investigate the effect of such planar defects on anisotropic growth, we used silver nanoplates as seeds. Silver nanoplates are enclosed by {111} facets on the two basal planes and a mixture of {100} facets, {111} facets, and planar defects on the sides (see Figure 5).[38,61−63] If planar defects do not significantly contribute to the growth rate on the side planes, the $R$ of silver nanoplates will be approximately the same as the $R$ of single-crystal silver nanoparticles and $R_j$ determined by electrochemical measurements (Figure 3B).


https://doi.org/10.1021/acs.chemmater.1c02474
Chem. Mater. 2021, 33, 8301−8311

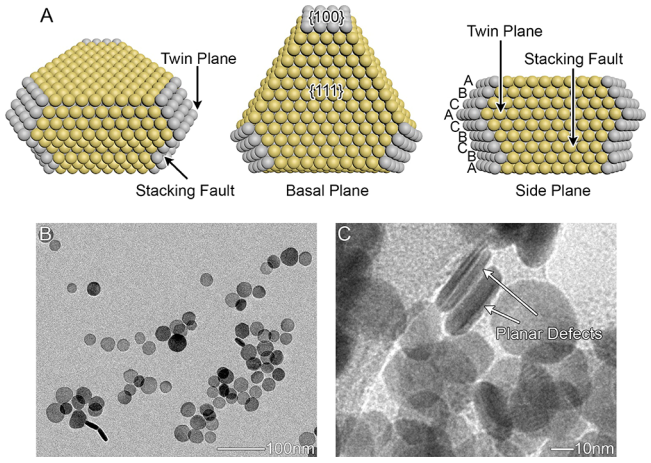


**Figure 5.** (A) Simplified schematic of the structure of silver nanoplates (nanodisks) in which the basal planes are {111} facets and the side planes contain a mixture of {100} facets, {111} facets, and planar defects. (B) TEM image of silver nanodisks and (C) HRTEM image of the planar defects in silver nanodisks.

Figure 6A shows a SEM image of the silver nanoplate seeds. UV−vis−NIR spectra for silver nanodisks and nanoplates are shown in Figure S7B. For the seed-mediated growth of silver nanoplates in a solution without citrate, the edge length of the silver nanoplates increased from 210 to 260 nm and the thickness increased from 9 to 70 nm. Thus, the ratio ($r$) between the growth in edge length and thickness is 0.82 without citrate (see Figure 6B and Figure S8A). Based on the geometry of silver nanoplates, the $R$ of silver nanoplates under this condition is 0.88 ($R$ = 1.061$r$; see Figure S9 and the associated discussion in the Supporting Information). This value of $R$ is close to the $R$ of single-crystal silver nanoparticles (0.87) and the $R_j$ from the electrochemical measurements (0.719), indicating that the presence of planar defects alone does not cause anisotropic growth.

Note that the silver nanoplates grown without citrate are thicker around the edges. The nanoplates grown in the 0.001 mM citrate solution also have thicker edges than the inner regions of the plates, but the nanoplates are larger and thinner, with an $R$ of 2.4 (Figure 6C and Figure S8B). When the citrate concentration is increased to 0.004 mM, the $R$ of the silver nanoplates increases to 26 (Figure 6D and Figure S8C). Under this condition, the nanoplates become uniform in thickness but the edges are not smooth and the shape is not well-defined. When the citrate concentration is increased to be greater than or equal to 0.007 mM, the nanoplates grow to be more triangular or hexagonal in shape with uniform thickness and smooth edges, and the $R$ of the silver nanoplates is over 45 (Figure 6E−H and Figures S8D−I and S10). The edge length increases and the thickness decreases as the citrate concentration is increased from 0.000 to 0.010 mM, but the edge length and thickness remain the same when the citrate concentration is increased from 0.01 to 0.45 mM (Figure 6I). As a result, the $R$ of silver nanoplates increases from 0.88 to

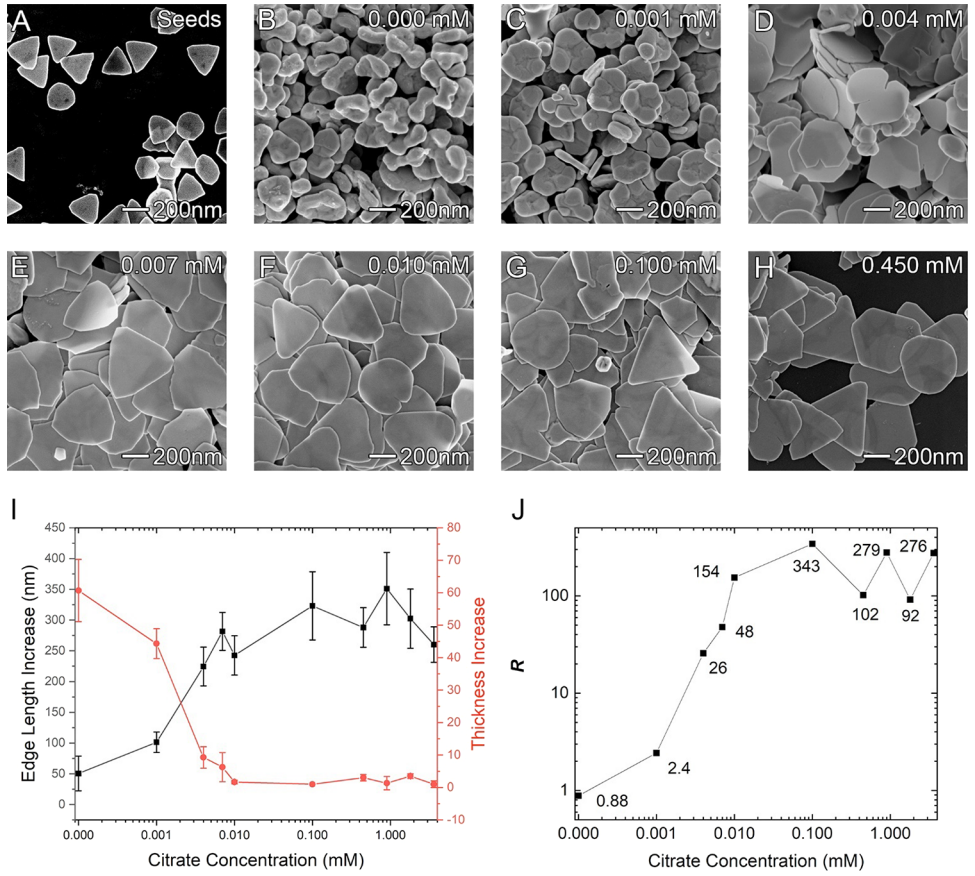


**Figure 6.** (A) SEM image of silver nanoplate seeds. (B−H) SEM images of silver nanoplates grown from the nanoplate seeds at citrate concentrations of (B) 0.000 mM, (C) 0.001 mM, (D) 0.004 mM, (E) 0.007 mM, (F) 0.010 mM, (G) 0.100 mM, and (H) 0.450 mM. (I) The edge length and thickness increase after growth at different citrate concentrations. (J) $R$ of silver nanoplates at different citrate concentrations.


https://doi.org/10.1021/acs.chemmater.1c02474
Chem. Mater. 2021, 33, 8301−8311

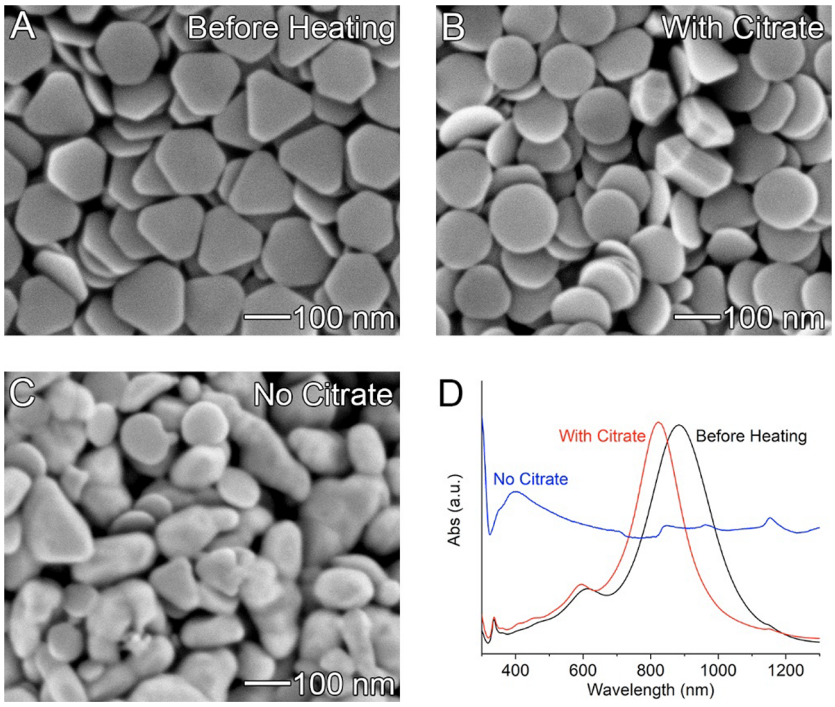


**Figure 7.** (A) SEM image of truncated triangular silver nanoplates before heating. (B) The nanoplates became nanodisks after heating with 0.45 mM citrate, 0.4 mM AA, and 1.15 mM trifluoroacetic acid in water at 95 °C for 10 min. (C) The nanoplates became spheroidal nanoparticles after heating in water with 0.4 mM AA, 0.25 mM trifluoroacetic acid, and 0.9 mM sodium trifluoroacetate at 95 °C for 10 min. The concentrations of trifluoroacetic acid and sodium trifluoroacetate were changed for different citrate concentrations to keep the pH = 3.6. (D) UV−vis−NIR spectra of suspensions of the nanostructures in A−C.

154 as the citrate concentration is increased from 0.000 to 0.010 mM (Figure 6J). The $R$ at citrate concentrations higher than 0.010 mM fluctuates between 90 and 350 because the increase in thickness is less than 2 nm, and this causes a small change in thickness to produce a large change in $R$.

The $R$ of single-crystal silver nanoparticles (0.87−1.73) is fairly close to the $R_j$ measured by electrochemical measurements under the same conditions (0.719−1.47), but the $R$ of silver nanoplates is clearly much larger than the $R_j$ in solutions containing more than 0.004 mM of citrate (26−343). These results suggest that citrate selectively passivating AA oxidation on the {111} facets of the nanoplates cannot by itself explain the much larger $R$ of nanoplates compared to single-crystal nanoparticles. Since the only difference between the single-crystal nanoparticles and the nanoplates is the presence of planar defects, these planar defects likely contribute to the large $R$ of silver nanoplates (Figure 6J). However, the results also indicate that stacking faults by themselves cannot drive anisotropic growth because the $R$ of silver nanoplates without citrate is 0.88, close to the $R$ of single-crystal silver nanoparticles (0.87) and the $R_j$ from the electrochemical measurements (0.719).

The thin middle and thick edges of nanoplates grown without citrate suggest that the planar defects are accelerating the deposition of silver atoms at the sides but that these atoms can then diffuse to the {111} surfaces on the top and bottom of the nanoplates. This diffusion creates a gradient of deposition that results in the thick edges and thin middle of the nanoplate. A possible explanation for the large anisotropic growth observed upon the addition of citrate may be that the addition of citrate slows the diffusion of atoms from the sides of the nanoplates to the top and bottom {111} surfaces. With this diffusion pathway blocked by citrate, the increased atomic deposition caused by the planar defects results in the deposition of silver primarily on the sides of the nanoplate, resulting in a much larger anisotropic growth than can be accounted for with the single-crystal electrochemistry measurements.

To test the hypothesis that citrate slows the diffusion of silver atoms to {111} facets, triangular silver nanoplates were heated at 95 °C in the presence or absence of citrate for 10 min. Before heating, the silver nanoplates were slightly truncated triangular nanoplates (Figure 7A). After heating with citrate, AA, and TFA at the same concentrations used to make the silver nanoplates in Figure 6H, the nanoplates became nanodisks (Figure 7B). However, the planar nature of the nanoplate, with large {111} facets on the top and bottom surfaces, was preserved. In contrast, if the truncated triangular nanoplates were heated with AA and TFA but no citrate, the shape of the particles became irregular and rounded (Figure 7C). Figure 7D shows that the absorption peak of the triangular nanoplates at 884 nm was shifted to 823 nm after heating with citrate, while the peak was shifted to 395 nm after heating without citrate. The small blueshift after heating with citrate indicates that the anisotropic shape of the nanoplate was largely preserved, whereas the large blueshift after heating without citrate confirms that the nanoplates morphed into spheroidal particles. Thus, the presence of citrate was necessary to prevent the diffusion of atoms to the large {111} planes and prevent the loss of the planar nanoplate shape. This result provides additional support for the hypothesis that the primary mechanism by which citrate enables the large anisotropic growth of nanoplates is that is slows the diffusion of atoms to {111} facets.


https://doi.org/10.1021/acs.chemmater.1c02474
Chem. Mater. 2021, 33, 8301−8311

## CONCLUSIONS

We used single-crystal electrodes to measure the extent to which citrate passivates (100) and (111) surfaces. Citrate decreased the rate of silver ion reduction to the same extent on Ag(100) and Ag(111) but decreased the rate of ascorbic acid oxidation to a greater extent (by 3.4 times) on Ag(111) than on Ag(100). Thus, we can conclude that citrate is a passivator and that the facet-selective effect of citrate on silver nanocrystal growth is due to citrate's facet-selective passivation of ascorbic acid oxidation. The concentration-dependent facet-selective passivation of citrate as measured with single-crystal electrodes is closely corroborated by the citrate-dependent anisotropic growth of single-crystal cuboctahedra into truncated cuboctahedra and octahedra, indicating that the facet-selective passivation measured with single-crystal electrodes can account for the anisotropic growth of single-crystal seeds. However, the anisotropic growth of seeds with planar defects is 30−100 times greater than can be accounted for with the single-crystal electrode measurements. Without citrate, seeds with planar defects exhibit greater deposition on their edges but do not exhibit anisotropic growth. This suggests that planar defects catalyze the deposition of silver but then the silver diffuses to {111} facets without citrate. Thus, planar defects increase the rate of silver deposition but do not by themselves contribute to anisotropic growth. Citrate may prevent the diffusion of the deposited silver to {111} facets, resulting in the much larger anisotropic growth than can be accounted for with the single-crystal electrode measurements. This hypothesis for the role of citrate is supported by observations that citrate preserves the planar nanoplate shape after heating. Without citrate, heating causes the nanoplates to become irregular and spheroidal.

Previous studies of anisotropic growth of pentagonally twinned gold nanorods, copper nanowires, and copper microplates with single-crystal electrodes have also reported that the extent of anisotropic growth of the nanocrystal with planar defects is more than 10 times larger than can be accounted for from the ratios of the currents measured on (100) and (111) single-crystal electrodes.[66−68] The difference in the extent of anisotropic growth observed for nanocrystals with planar defects and from measurements with single-crystal electrodes may be due to a similar effect as that observed in this work, i.e., that planar defects catalyze atomic deposition. Additional comparisons of the anisotropic growth of single-crystal seeds and seeds with planar defects under identical conditions, with accompanying single-crystal electrode measurements, may shed light on the extent to which planar defects catalyze atomic deposition for gold, copper, and palladium nanocrystals. Quantifying the effects of additives and planar defects on the extent of anisotropic growth is important for designing nanocrystal synthesis to produce a desired shape.

## ASSOCIATED CONTENT

### Supporting Information

The Supporting Information is available free of charge at https://pubs.acs.org/doi/10.1021/acs.chemmater.1c02474.

Assignments of measured current densities to chemical processes, determination of $R$ for a nanoplate based on its dimensional change, verification of the single-crystal electrode facets, TEM images of the seeds, schematic representations and dimensional measurements of different types of nanocrystals, additional LSV measurements, additional SEM images of the silver nanoplates, and additional details about experimental measurements (PDF)

## AUTHOR INFORMATION


### Corresponding Author

**Benjamin J. Wiley** − *Department of Chemistry, Duke University, Durham, North Carolina 27708, United States;* orcid.org/0000-0002-1314-6223; Email: benjamin.wiley@duke.edu

### Author

**Heng Xu** − *Department of Chemistry, Duke University, Durham, North Carolina 27708, United States;* orcid.org/0000-0002-8259-5516

Complete contact information is available at: https://pubs.acs.org/10.1021/acs.chemmater.1c02474


### Notes

The authors declare no competing financial interest.

## ACKNOWLEDGMENTS

This work was supported by NSF Grant CHE-1808108. SEM, TEM, and UV−vis−NIR spectroscopy were performed at the Duke University Shared Materials Instrumentation Facility (SMIF), a member of the North Carolina Research Triangle Nanotechnology Network (RTNN), which is supported by the National Science Foundation (award ECCS-2025064) as part of the National Nanotechnology Coordinated Infrastructure (NNCI).

## REFERENCES


(1) Liu, L.; Corma, A. Metal Catalysts for Heterogeneous Catalysis: From Single Atoms to Nanoclusters and Nanoparticles. *Chem. Rev.* **2018**, *118*, 4981−5079.

(2) Li, Z.; Fu, J.-Y.; Feng, Y.; Dong, C.-K.; Liu, H.; Du, X.-W. A silver catalyst activated by stacking faults for the hydrogen evolution reaction. *Nat. Catal.* **2019**, *2*, 1107−1114.

(3) Zhou, K.; Li, Y. Catalysis Based on Nanocrystals with Well-Defined Facets. *Angew. Chem., Int. Ed.* **2012**, *51*, 602−613.

(4) Xie, S.; Choi, S.-I.; Xia, X.; Xia, Y. Catalysis on faceted noble-metal nanocrystals: both shape and size matter. *Curr. Opin. Chem. Eng.* **2013**, *2*, 142−150.

(5) Shi, Y.; Lyu, Z.; Zhao, M.; Chen, R.; Nguyen, Q. N.; Xia, Y. Noble-Metal Nanocrystals with Controlled Shapes for Catalytic and Electrocatalytic Applications. *Chem. Rev.* **2021**, *121*, 649−735.

(6) Mulvihill, M. J.; Ling, X. Y.; Henzie, J.; Yang, P. Anisotropic Etching of Silver Nanoparticles for Plasmonic Structures Capable of Single-Particle SERS. *J. Am. Chem. Soc.* **2010**, *132*, 268−274.

(7) Zhang, Q.; Moran, C. H.; Xia, X.; Rycenga, M.; Li, N.; Xia, Y. Synthesis of Ag Nanobars in the Presence of Single-Crystal Seeds and a Bromide Compound, and Their Surface-Enhanced Raman Scattering (SERS) Properties. *Langmuir* **2012**, *28*, 9047−9054.

(8) Abdulhalim, I. Plasmonic Sensing Using Metallic Nano-Sculptured Thin Films. *Small* **2014**, *10*, 3499−3514.

(9) Gao, C.; Lu, Z.; Liu, Y.; Zhang, Q.; Chi, M.; Cheng, Q.; Yin, Y. Highly Stable Silver Nanoplates for Surface Plasmon Resonance Biosensing. *Angew. Chem., Int. Ed.* **2012**, *51*, 5629−5633.

(10) Sannicolo, T.; Lagrange, M.; Cabos, A.; Celle, C.; Simonato, J. P.; Bellet, D. Metallic Nanowire-Based Transparent Electrodes for Next Generation Flexible Devices: a Review. *Small* **2016**, *12*, 6052−6075.

(11) Hecht, D. S.; Hu, L.; Irvin, G. Emerging Transparent Electrodes Based on Thin Films of Carbon Nanotubes, Graphene, and Metallic Nanostructures. *Adv. Mater.* **2011**, *23*, 1482−1513.

(12) Huo, D.; Kim, M. J.; Lyu, Z.; Shi, Y.; Wiley, B. J.; Xia, Y. One-Dimensional Metal Nanostructures: From Colloidal Syntheses to Applications. *Chem. Rev.* **2019**, *119*, 8972−9073.
(13) Kumar, A.; Kim, S.; Nam, J.-M. Plasmonically Engineered Nanoprobes for Biomedical Applications. *J. Am. Chem. Soc.* **2016**, *138*, 14509−14525.
(14) Bhattacharya, R.; Mukherjee, P. Biological properties of "naked" metal nanoparticles. *Adv. Drug Delivery Rev.* **2008**, *60*, 1289−1306.
(15) Dreaden, E. C.; El-Sayed, M. A. Detecting and Destroying Cancer Cells in More than One Way with Noble Metals and Different Confinement Properties on the Nanoscale. *Acc. Chem. Res.* **2012**, *45*, 1854−1865.
(16) Jin, R.; Cao, Y.; Mirkin, C. A.; Kelly, K. L.; Schatz, G. C.; Zheng, J. G. Photoinduced conversion of silver nanospheres to nanoprisms. *Science* **2001**, *294*, 1901−1903.
(17) Homan, K. A.; Souza, M.; Truby, R.; Luke, G. P.; Green, C.; Vreeland, E.; Emelianov, S. Silver Nanoplate Contrast Agents for in Vivo Molecular Photoacoustic Imaging. *ACS Nano* **2012**, *6*, 641−650.
(18) Niu, Z.; Cui, F.; Kuttner, E.; Xie, C.; Chen, H.; Sun, Y.; Dehestani, A.; Schierle-Arndt, K.; Yang, P. Synthesis of Silver Nanowires with Reduced Diameters Using Benzoin-Derived Radicals to Make Transparent Conductors with High Transparency and Low Haze. *Nano Lett.* **2018**, *18*, 5329−5334.
(19) Mutiso, R. M.; Sherrott, M. C.; Rathmell, A. R.; Wiley, B. J.; Winey, K. I. Integrating Simulations and Experiments To Predict Sheet Resistance and Optical Transmittance in Nanowire Films for Transparent Conductors. *ACS Nano* **2013**, *7*, 7654−7663.
(20) Li, B.; Ye, S.; Stewart, I. E.; Alvarez, S.; Wiley, B. J. Synthesis and Purification of Silver Nanowires To Make Conducting Films with a Transmittance of 99%. *Nano Lett.* **2015**, *15*, 6722−6726.
(21) Ye, S.; Rathmell, A. R.; Chen, Z.; Stewart, I. E.; Wiley, B. J. Metal Nanowire Networks: The Next Generation of Transparent Conductors. *Adv. Mater.* **2014**, *26*, 6670−6687.
(22) Bergin, S. M.; Chen, Y.-H.; Rathmell, A. R.; Charbonneau, P.; Li, Z.-Y.; Wiley, B. J. The effect of nanowire length and diameter on the properties of transparent, conducting nanowire films. *Nanoscale* **2012**, *4*, 1996−2004.
(23) Khanarian, G.; Joo, J.; Liu, X.-Q.; Eastman, P.; Werner, D.; O'Connell, K.; Trefonas, P. The optical and electrical properties of silver nanowire mesh films. *J. Appl. Phys.* **2013**, *114*, No. 024302.
(24) Christopher, P.; Linic, S. Engineering Selectivity in Heterogeneous Catalysis: Ag Nanowires as Selective Ethylene Epoxidation Catalysts. *J. Am. Chem. Soc.* **2008**, *130*, 11264−11265.
(25) Christopher, P.; Linic, S. Shape- and Size-Specific Chemistry of Ag Nanostructures in Catalytic Ethylene Epoxidation. *ChemCatChem* **2010**, *2*, 78−83.
(26) Kuo, T.-R.; Lee, Y.-C.; Chou, H.-L.; Swathi, M. G.; Wei, C.-Y.; Wen, C.-Y.; Chang, Y.-H.; Pan, X.-Y.; Wang, D.-Y. Plasmon-Enhanced Hydrogen Evolution on Specific Facet of Silver Nanocrystals. *Chem. Mater.* **2019**, *31*, 3722−3728.
(27) Yang, T.-H.; Shi, Y.; Janssen, A.; Xia, Y. Surface Capping Agents and Their Roles in Shape-Controlled Synthesis of Colloidal Metal Nanocrystals. *Angew. Chem., Int. Ed.* **2020**, *59*, 15378−15401.
(28) Xia, Y.; Xiong, Y.; Lim, B.; Skrabalak, S. E. Shape-Controlled Synthesis of Metal Nanocrystals: Simple Chemistry Meets Complex Physics? *Angew. Chem., Int. Ed.* **2009**, *48*, 60−103.
(29) Wiley, B.; Sun, Y.; Mayers, B.; Xia, Y. Shape-Controlled Synthesis of Metal Nanostructures: The Case of Silver. *Chem. − Eur. J.* **2005**, *11*, 454−463.
(30) Xia, Y.; Xia, X.; Peng, H.-C. Shape-Controlled Synthesis of Colloidal Metal Nanocrystals: Thermodynamic versus Kinetic Products. *J. Am. Chem. Soc.* **2015**, *137*, 7947−7966.
(31) Lohse, S. E.; Burrows, N. D.; Scarabelli, L.; Liz-Marzán, L. M.; Murphy, C. J. Anisotropic Noble Metal Nanocrystal Growth: The Role of Halides. *Chem. Mater.* **2014**, *26*, 34−43.
(32) Ghosh, S.; Manna, L. The Many "Facets" of Halide Ions in the Chemistry of Colloidal Inorganic Nanocrystals. *Chem. Rev.* **2018**, *118*, 7804−7864.
(33) Zeng, J.; Zheng, Y.; Rycenga, M.; Tao, J.; Li, Z.-Y.; Zhang, Q.; Zhu, Y.; Xia, Y. Controlling the Shapes of Silver Nanocrystals with Different Capping Agents. *J. Am. Chem. Soc.* **2010**, *132*, 8552−8553.
(34) Langille, M. R.; Personick, M. L.; Zhang, J.; Mirkin, C. A. Defining Rules for the Shape Evolution of Gold Nanoparticles. *J. Am. Chem. Soc.* **2012**, *134*, 14542−14554.
(35) Chen, Z.; Balankura, T.; Fichthorn, K. A.; Rioux, R. M. Revisiting the Polyol Synthesis of Silver Nanostructures: Role of Chloride in Nanocube Formation. *ACS Nano* **2019**, *13*, 1849−1860.
(36) Wang, Z. L. Transmission Electron Microscopy of Shape-Controlled Nanocrystals and Their Assemblies. *J. Phys. Chem. B* **2000**, *104*, 1153−1175.
(37) Sun, Y.; Xia, Y. Shape-controlled synthesis of gold and silver nanoparticles. *Science* **2002**, *298*, 2176−2179.
(38) Zhang, Q.; Li, N.; Goebl, J.; Lu, Z.; Yin, Y. A Systematic Study of the Synthesis of Silver Nanoplates: Is Citrate a "Magic" Reagent? *J. Am. Chem. Soc.* **2011**, *133*, 18931−18939.
(39) Wiley, B.; Sun, Y.; Chen, J.; Cang, H.; Li, Z.-Y.; Li, X.; Xia, Y. Shape-Controlled Synthesis of Silver and Gold Nanostructures. *MRS Bull.* **2005**, *30*, 356−361.
(40) Sun, Y.; Mayers, B.; Herricks, T.; Xia, Y. Polyol Synthesis of Uniform Silver Nanowires: A Plausible Growth Mechanism and the Supporting Evidence. *Nano Lett.* **2003**, *3*, 955−960.
(41) Johnson, C. J.; Dujardin, E.; Davis, S. A.; Murphy, C. J.; Mann, S. Growth and form of gold nanorods prepared by seed-mediated, surfactant-directed synthesis. *J. Mater. Chem.* **2002**, *12*, 1765−1770.
(42) Sau, T. K.; Murphy, C. J. Room Temperature, High-Yield Synthesis of Multiple Shapes of Gold Nanoparticles in Aqueous Solution. *J. Am. Chem. Soc.* **2004**, *126*, 8648−8649.
(43) González-Rubio, G.; Scarabelli, L.; Guerrero-Martínez, A.; Liz-Marzán, L. M. Surfactant-Assisted Symmetry Breaking in Colloidal Gold Nanocrystal Growth. *ChemNanoMat* **2020**, *6*, 698−707.
(44) Qi, X.; Fichthorn, K. A. Theory of the thermodynamic influence of solution-phase additives in shape-controlled nanocrystal synthesis. *Nanoscale* **2017**, *9*, 15635−15642.
(45) Cha, M. G.; Kang, H.; Choi, Y.-S.; Cho, Y.; Lee, M.; Lee, H.-Y.; Lee, Y.-S.; Jeong, D. H. Effect of Alkylamines on Morphology Control of Silver Nanoshells for Highly Enhanced Raman Scattering. *ACS Appl. Mater. Interfaces* **2019**, *11*, 8374−8381.
(46) Ou, W.; Shen, J.; Lyu, F.; Xiao, X.; Zhou, B.; Lu, J.; Li, Y. Y. Facile Surfactant-, Reductant-, and Ag Salt-free Growth of Ag Nanoparticles with Controllable Size from 35 to 660 nm on Bulk Ag Materials. *Chem. − Asian J.* **2021**, *16*, 2249−2252.
(47) Merkoçi, F.; Patarroyo, J.; Russo, L.; Piella, J.; Genç, A.; Arbiol, J.; Bastús, N. G.; Puntes, V. Understanding galvanic replacement reactions: the case of Pt and Ag. *Mater. Today Adv.* **2020**, *5*, 100037.
(48) Smith, D. K.; Miller, N. R.; Korgel, B. A. Iodide in CTAB Prevents Gold Nanorod Formation. *Langmuir* **2009**, *25*, 9518−9524.
(49) Rayavarapu, R. G.; Ungureanu, C.; Krystek, P.; van Leeuwen, T. G.; Manohar, S. Iodide Impurities in Hexadecyltrimethylammonium Bromide (CTAB) Products: Lot−Lot Variations and Influence on Gold Nanorod Synthesis. *Langmuir* **2010**, *26*, 5050−5055.
(50) Millstone, J. E.; Wei, W.; Jones, M. R.; Yoo, H.; Mirkin, C. A. Iodide Ions Control Seed-Mediated Growth of Anisotropic Gold Nanoparticles. *Nano Lett.* **2008**, *8*, 2526−2529.
(51) Lohse, S. E.; Murphy, C. J. The Quest for Shape Control: A History of Gold Nanorod Synthesis. *Chem. Mater.* **2013**, *25*, 1250−1261.
(52) DuChene, J. S.; Niu, W.; Abendroth, J. M.; Sun, Q.; Zhao, W.; Huo, F.; Wei, W. D. Halide Anions as Shape-Directing Agents for Obtaining High-Quality Anisotropic Gold Nanostructures. *Chem. Mater.* **2013**, *25*, 1392−1399.
(53) Ye, X.; Jin, L.; Caglayan, H.; Chen, J.; Xing, G.; Zheng, C.; Doan-Nguyen, V.; Kang, Y.; Engheta, N.; Kagan, C. R.; Murray, C. B. Improved Size-Tunable Synthesis of Monodisperse Gold Nanorods through the Use of Aromatic Additives. *ACS Nano* **2012**, *6*, 2804−2817.


https://doi.org/10.1021/acs.chemmater.1c02474
*Chem. Mater.* 2021, 33, 8301−8311

(54) Wiley, B.; Sun, Y.; Xia, Y. Polyol Synthesis of Silver Nanostructures: Control of Product Morphology with Fe(II) or Fe(III) Species. *Langmuir* **2005**, *21*, 8077−8080.
(55) Xiong, Y.; Chen, J.; Wiley, B.; Xia, Y.; Aloni, S.; Yin, Y. Understanding the Role of Oxidative Etching in the Polyol Synthesis of Pd Nanoparticles with Uniform Shape and Size. *J. Am. Chem. Soc.* **2005**, *127*, 7332−7333.
(56) Skrabalak, S. E.; Wiley, B. J.; Kim, M.; Formo, E. V.; Xia, Y. On the Polyol Synthesis of Silver Nanostructures: Glycolaldehyde as a Reducing Agent. *Nano Lett.* **2008**, *8*, 2077−2081.
(57) Li, H.; Xia, H.; Wang, D.; Tao, X. Simple Synthesis of Monodisperse, Quasi-spherical, Citrate-Stabilized Silver Nanocrystals in Water. *Langmuir* **2013**, *29*, 5074−5079.
(58) Pietrobon, B.; McEachran, M.; Kitaev, V. Synthesis of Size-Controlled Faceted Pentagonal Silver Nanorods with Tunable Plasmonic Properties and Self-Assembly of These Nanorods. *ACS Nano* **2009**, *3*, 21−26.
(59) Kilin, D. S.; Prezhdo, O. V.; Xia, Y. Shape-controlled synthesis of silver nanoparticles: Ab initio study of preferential surface coordination with citric acid. *Chem. Phys. Lett.* **2008**, *458*, 113−116.
(60) Tang, Z.; Zhang, Q.; Yin, Y.; Chang, C.-e. A. Facet Selectivity of Ligands on Silver Nanoplates: Molecular Mechanics Study. *J. Phys. Chem. C* **2014**, *118*, 21589−21598.
(61) Zeng, J.; Tao, J.; Li, W.; Grant, J.; Wang, P.; Zhu, Y.; Xia, Y. A Mechanistic Study on the Formation of Silver Nanoplates in the Presence of Silver Seeds and Citric Acid or Citrate Ions. *Chem. − Asian J.* **2011**, *6*, 376−379.
(62) Germain, V.; Li, J.; Ingert, D.; Wang, Z. L.; Pileni, M. P. Stacking Faults in Formation of Silver Nanodisks. *J. Phys. Chem. B* **2003**, *107*, 8717−8720.
(63) Aherne, D.; Ledwith, D. M.; Gara, M.; Kelly, J. M. Optical Properties and Growth Aspects of Silver Nanoprisms Produced by a Highly Reproducible and Rapid Synthesis at Room Temperature. *Adv. Funct. Mater.* **2008**, *18*, 2005−2016.
(64) Kim, M. J.; Brown, M.; Wiley, B. J. Electrochemical investigations of metal nanostructure growth with single crystals. *Nanoscale* **2019**, *11*, 21709−21723.
(65) Kim, M. J.; Flowers, P. F.; Stewart, I. E.; Ye, S.; Baek, S.; Kim, J. J.; Wiley, B. J. Ethylenediamine Promotes Cu Nanowire Growth by Inhibiting Oxidation of Cu(111). *J. Am. Chem. Soc.* **2017**, *139*, 277−284.
(66) Kim, M. J.; Alvarez, S.; Chen, Z.; Fichthorn, K. A.; Wiley, B. J. Single-Crystal Electrochemistry Reveals Why Metal Nanowires Grow. *J. Am. Chem. Soc.* **2018**, *140*, 14740−14746.
(67) Kim, M. J.; Cruz, M. A.; Chen, Z.; Xu, H.; Brown, M.; Fichthorn, K. A.; Wiley, B. J. Isotropic Iodide Adsorption Causes Anisotropic Growth of Copper Microplates. *Chem. Mater.* **2021**, *33*, 881−891.
(68) Brown, M.; Wiley, B. J. Bromide Causes Facet-Selective Atomic Addition in Gold Nanorod Syntheses. *Chem. Mater.* **2020**, *32*, 6410−6415.
(69) Skrabalak, S. E.; Au, L.; Li, X.; Xia, Y. Facile synthesis of Ag nanocubes and Au nanocages. *Nat. Protoc.* **2007**, *2*, 2182−2190.
(70) Zhang, Q.; Li, W.; Wen, L.-P.; Chen, J.; Xia, Y. Facile Synthesis of Ag Nanocubes of 30 to 70 nm in Edge Length with CF3COOAg as a Precursor. *Chem. − Eur. J.* **2010**, *16*, 10234−10239.
(71) Mushran, S. P.; Agrawal, M. C.; Mehrotra, R. M.; Sanehi, R. Kinetics and mechanism of reduction of silver(I) by ascorbic acid. *J. Chem. Soc., Dalton Trans.* **1974**, 1460−1462.
(72) Lastraioli, E.; Loglio, F.; Cavallini, M.; Simeone, F. C.; Innocenti, M.; Carlà, F.; Foresti, M. L. In Situ Scanning Tunneling Microscopy Investigation of Sulfur Oxidative Underpotential Deposition on Ag(100) and Ag(110). *Langmuir* **2010**, *26*, 17679−17685.
(73) Hatchett, D. W.; White, H. S. Electrochemistry of Sulfur Adlayers on the Low-Index Faces of Silver. *J. Phys. Chem.* **1996**, *100*, 9854−9859.
(74) Perez, N., *Electrochemistry and Corrosion Science*; Kluwer Academic Publishers: Boston, MA, 2004, 155−158.
(75) Xiong, Y.; Washio, I.; Chen, J.; Sadilek, M.; Xia, Y. Trimeric Clusters of Silver in Aqueous AgNO3 Solutions and Their Role as Nuclei in Forming Triangular Nanoplates of Silver. *Angew. Chem., Int. Ed.* **2007**, *46*, 4917−4921.
(76) Jiang, X. C.; Chen, C. Y.; Chen, W. M.; Yu, A. B. Role of Citric Acid in the Formation of Silver Nanoplates through a Synergistic Reduction Approach. *Langmuir* **2010**, *26*, 4400−4408.


https://doi.org/10.1021/acs.chemmater.1c02474
*Chem. Mater.* 2021, 33, 8301−8311